# Dual-Band Microstrip Bandpass Filter Using Stepped-Impedance Resonators With New Coupling Schemes

Yue Ping Zhang and Mei Sun

***Abstract*—A microstrip bandpass filter using stepped-impedance resonators is designed in low-temperature co-fired ceramic technology for dual-band applications at 2.4 and 5.2 GHz. New coupling schemes are proposed to replace the normal counterparts. It is found that the new coupling scheme for the interstages can enhance the layout compactness of the bandpass filter; while the new coupling scheme at the input and output can improve the performance of the bandpass filter. To validate the design and analysis, a prototype of the bandpass filter was fabricated and measured. It is shown that the measured and simulated performances are in good agreement. The prototype of the bandpass filter achieved insertion loss of 1.25 and 1.87 dB, $S_{11}$ of $-29$ and $-40$ dB, and bandwidth of 21% and 12.7% at 2.4 and 5.2 GHz, respectively. The bandpass filter is further studied for a single-package solution of dual-band radio transceivers. The bandpass filter is, therefore, integrated into a ceramic ball grid array package. The integration is analyzed with an emphasis on the connection of the bandpass filter to the antenna and to the transceiver die.**

***Index Terms*—Dual-band filter, low-temperature co-fired ceramic (LTCC), microstrip, stepped-impedance resonator.**

## I. Introduction

A DUAL-BAND filter is a key component of a radio transceiver in a dual-band wireless communication system. Intuitively, a dual-band filter can be realized with the combination of two single-band filters. However, this approach not only consumes twice the size of a single-band filter, but also requires additional external combining networks [1]. Guo *et al.* have redesigned the two single-band filters so that one filter has a low-pass and the other a high-pass characteristic, thus one filter is open in the passband of the other, and as a result, there is no need of additional combining networks [2]. Alternatively, the dual-band filter can be realized using resonators that consist of open or short stubs in parallel or in series to create two passbands with three transmission zeros. Quendo *et al.* first showed that three parallel open stubs are needed [3]; while Lee *et al.* demonstrated that only two parallel open stubs are enough to behave as a resonator with dual-band properties [4]. Tsai *et al.* extended from parallel open to series open stubs and also found that filters with short stubs are duals of the ones with open stubs [5]. The parameters of their duals can be easily obtained by using the duality transformations. Recently, more and more dual-band filters have been realized with stepped-impedance resonators [6]–[8] because of their dual-band behavior, simple structures, and well-established design methodology [9]. In this paper, we also report on a dual-band filter using stepped-impedance resonators with the new coupling schemes. It is found that the new coupling schemes can improve both the layout compactness and performance of the dual-band filter. More importantly, the dual-band filter is further studied for a single-package solution of dual-band radio transceivers [10]. The dual-band filter is, therefore, integrated into a ceramic ball grid array package. The integration is analyzed with an emphasis on the connection of the dual-band filter to the antenna and transceiver die.

Manuscript received March 22, 2006; revised June 19, 2006.

The authors are with the Integrated Systems Research Laboratory, School of Electrical and Electronic Engineering, Nanyang Technological University, Singapore 639798 (e-mail: eypzhang@ntu.edu.sg; SUNM0001@ntu.edu.sg).

Digital Object Identifier 10.1109/TMTT.2006.882895

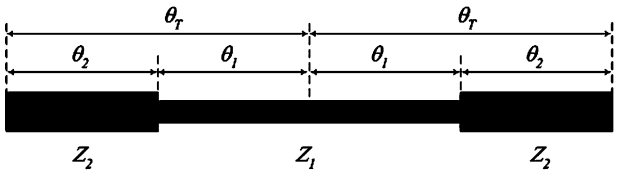


Fig. 1. Basic structure of the $\lambda/2$ stepped-impedance resonator.

## II. Dual-Band Microstrip Bandpass Filter Using Half-Wavelength Stepped-Impedance Resonators

The basic structure of a half-wavelength $(\lambda/2)$ microstrip stepped-impedance resonator is shown in Fig. 1. It consists of two lines of different characteristic impedance $Z_1$ and $Z_2$ and of electrical lengths $\theta_1$ and $\theta_2$ [9]. For practical application, $\theta_1$ is often chosen to be equal to $\theta_2$. The fundamental resonance occurs at

$$R_z = \tan^2 \theta_o \tag{1}$$

where $R_z$ is the ratio of characteristic impedance $Z_2$ to $Z_1$ and $\theta_o$ is the electrical length for the fundamental frequency at $f_o$. The first spurious resonance occurs at

$$\tan \theta_{s1} = \infty \tag{2}$$

where $\theta_{s1}$ is the electrical length for the first spurious frequency at $f_{s1}$. From (1) and (2), we obtain

$$\frac{f_{s1}}{f_o} = \frac{\theta_{s1}}{\theta_o} = \frac{\pi}{2\tan^{-1}\sqrt{R_z}}. \tag{3}$$

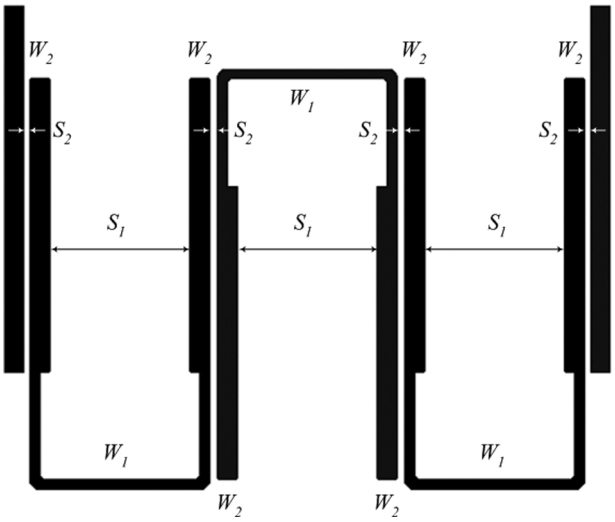


Fig. 2. Novel miniaturized dual-band bandpass filter where $W_1 = 0.236$ mm, $W_2 = 0.47$ mm, $S_1 = 3.6$ mm, and $S_2 = 0.189$ mm, and the whole footprint $< 15 \times 13$ mm$^2$.

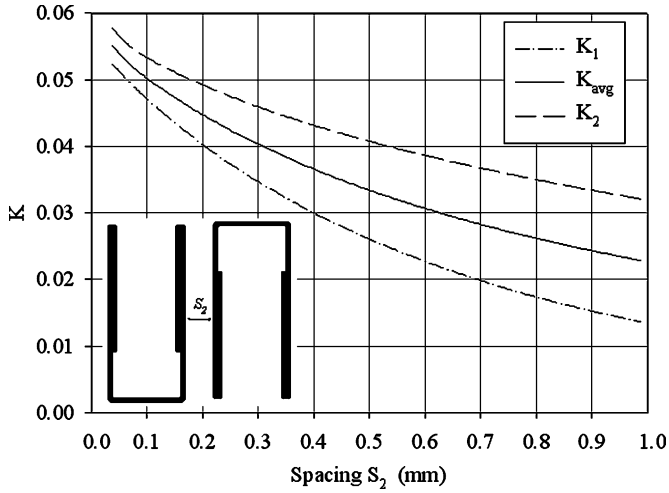


Fig. 3. Simulated coupling coefficient as a function of spacing between two resonators.

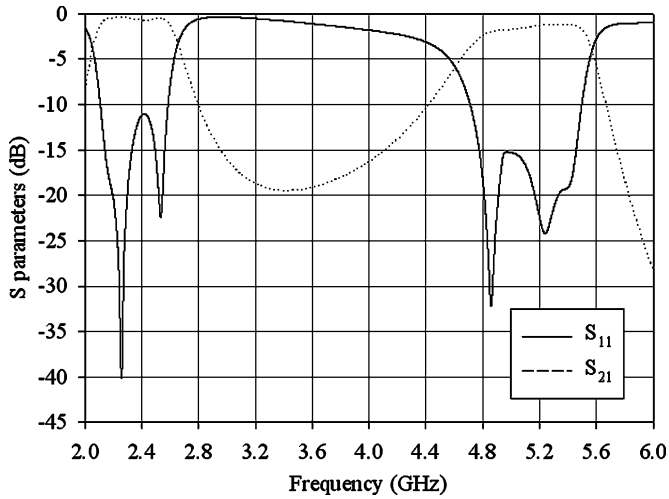


Fig. 4. Simulated frequency responses of the miniaturized dual-band bandpass filter.

It is clear from (3) that the spurious response can be controlled by the characteristic impedance ratio $R_z$. In this design, we set $f_o$ and $f_{s1}$ to be 2.4 and 5.2 GHz, respectively.

### A. Miniaturization

Fig. 2 shows the layout of the dual-band bandpass filter using three $\lambda/2$ stepped-impedance resonators on a low-temperature co-fired ceramic (LTCC) substrate of 1.0-mm thickness and with a dielectric constant of 7.8 and a loss tangent of 0.002. It is seen that the basic stepped-impedance resonator structure is configured to a hairpin structure. In the normal layout of the bandpass filter using stepped-impedance resonators of the hairpin structure, only the $Z_2$ sections are used for coupling [9]. In this design, both $Z_1$ and $Z_2$ sections are used for coupling. It is found that this new coupling scheme shifts down the central frequencies of the dual-band bandpass filter because the additional capacitance is introduced through the internal coupling of each resonator. As a result, the layout is more compact. The formulas given in [9] remain accurate for the calculation of $W_1$ and $W_2$ values as long as the internal spacing $S_1 \gg W_2$. However, they obviously become invalid for the calculation of the spacing $S_2$ between resonators. The required spacing between the resonators is related to the coupling coefficient $K$. Fig. 3 shows the simulated coupling coefficient as a function of $S_2$. It is evident that the coupling coefficient at 2.4 GHz $(K_1)$ is smaller than that at 5.2 GHz $(K_2)$ at a given spacing. Therefore, in order to obtain a similar performance at both frequencies, the average coupling coefficient value $(K_{\text{avg}})$ should be used. From the calculated coupling coefficient determined by the fractional bandwidth $\Delta$ of 0.06 and the passband ripple $R$ of 0.5 dB, the required spacing is found with the help of Fig. 3. For simplicity, we choose $S_2 = 0.189$ mm for all stages in Fig. 2.

Fig. 4 shows the simulated $S_{11}$ and $S_{21}$ of the dual-band bandpass filter. It is seen that the required central frequencies, relative bandwidths, and matching $(S_{11})$ are satisfied. However, the insertion loss $(S_{21})$ value is more than 2 dB at the 5.2-GHz band, which is too high for a dual-band radio transceiver. Hence, in Section II-B, we shall focus on the insertion loss enhancement of the dual-band bandpass filter, particularly at the 5.2-GHz band.

### B. Performance Enhancement

There are three major contributors to the insertion loss of the filter. They are the conductive, dielectric, and interstage coupling losses. The conductive loss is due to the finite conductivity of the conducting material, the dielectric loss is due to the nonzero loss tangent of the dielectric substrate, and the coupling loss is due to the power loss associated with the coupling between resonators. Both conductive and dielectric losses are affected by the material properties, which are fixed in the design. The coupling loss, however, is affected by the coupling structure, which is design dependent. Thus, an effective coupling scheme is an important design consideration for filters. Parallel-coupled sections are used in the miniaturized bandpass filter to realize coupling. One can narrow the spacing of the two adjacent parallel-coupled sections to obtain tighter coupling to

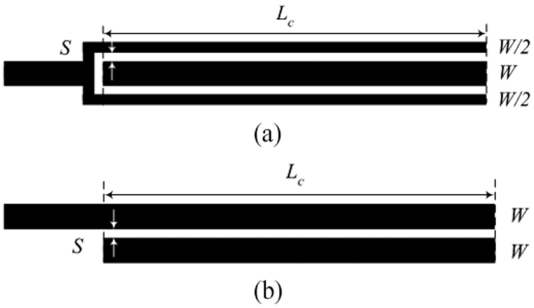


Fig. 5. Coupling schemes. (a) Novel. (b) Normal.

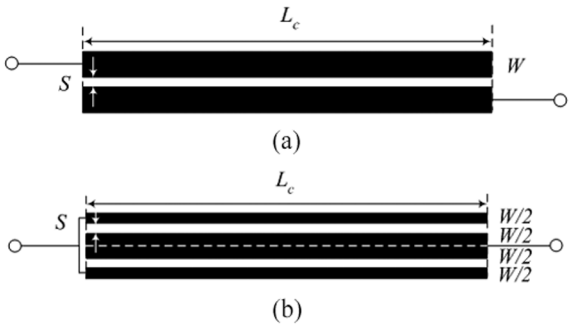


Fig. 6. Parallel-coupled microstrip lines. (a) Two. (b) Three.

achieve the required coupling strength. However, there is a minimum spacing between two adjacent conductors set by the fabrication technology. With the current LTCC fabrication technology, the minimum spacing is approximately 0.1 mm for mass production. Therefore, in order to achieve tighter coupling with this minimum spacing, we have created a new coupling scheme. Note that the new coupling scheme, as shown in Fig. 5(a), is realized by dividing the input line in the normal coupling scheme, as shown in Fig. 5(b), into two lines of a dual-finger structure. It is known that a line with characteristic impedance $Z_0$ can be represented as a parallel connection of two lines with characteristic impedance $2Z_0$. Therefore, under condition $Z_2' = 2Z_2$ and equal length, this new coupling scheme is electrically equivalent to the normal coupling scheme from the input to the direct port. However, it introduces tighter coupling from the input to the coupled port and, thus, lower the insertion loss. This is proven as follows using the theory of transmission line.

First consider two parallel-coupled microstrip lines shown in Fig. 6(a) for the normal coupling scheme. The equivalent circuit of the parallel-coupled microstrip lines can be expressed as a $J$-inverter susceptance $(J)$ and the two equal electrical lengths $(\theta/2)$ with characteristic admittance $Y_0$ [8]. The $J$-inverter susceptance is useful for design and optimization using the network-based synthesis technique and is directly proportional to the coupling strength of the pair of parallel-coupled microstrip lines [11]. As the characteristic impedances $(Z_{0e}, Z_{0o})$ and phase constants $(\beta_e, \beta_o)$ of the even and odd dominant modes of the pair of parallel-coupled microstrip lines can be calculated, the impedance $(Z)$ matrix defined for the input and

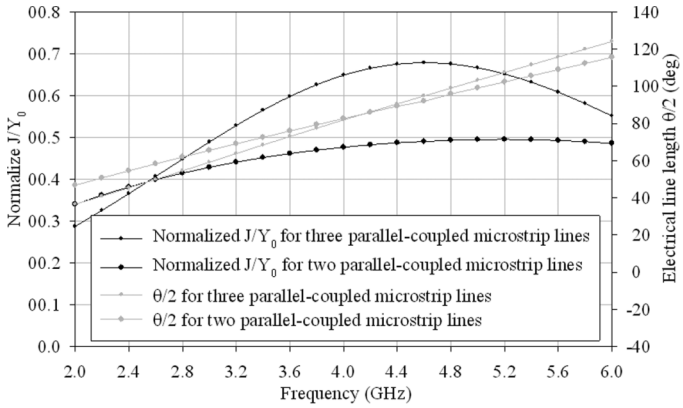


Fig. 7. $J$-inverter network parameters of the two and three parallel-coupled microstrip lines.

coupled ports of the pair of parallel-coupled microstrip lines can be written as

$$Z_{11} = Z_{22} = \frac{-j}{2}(Z_{0e}\cot\beta_e L_c + Z_{0o}\cot\beta_o L_c) \quad (4)$$

$$Z_{12} = Z_{21} = \frac{-j}{2}(Z_{0e}\csc\beta_e L_c - Z_{0o}\csc\beta_o L_c) \quad (5)$$

where each element is purely imaginary, and they can be converted into the admittance $(Y)$ matrix with the self-susceptance $B_{11} = B_{22}$ and mutual susceptance $B_{12} = B_{21}$. Under the network equivalence, the two $J$-inverter network elements susceptance $(J)$ and electrical length $(\theta)$ can be expressed as

$$\overline{J} = \frac{J}{Y_0} = \frac{\tan(\theta/2) - \overline{B}_{11}}{\overline{B}_{12}\tan(\theta/2)} \quad (6)$$

$$\theta = n\pi + \tan^{-1}\left(\frac{2\overline{B}_{11}}{1 - \overline{B}_{11}^2 + \overline{B}_{12}^2}\right) \quad (7)$$

where $\overline{B}_{11} = B_{11}/Y_0$, $\overline{B}_{12} = B_{12}/Y_0$, and $n$ is an integer.

Now consider three parallel-coupled microstrip lines shown in Fig. 6(b) for the new coupling scheme. Imagine that the middle line of width $W$ is divided into two lines of each width $W/2$. Thus, the three parallel-coupled microstrip lines for the new coupling scheme can be treated as a parallel connection of two pairs of the two parallel-coupled microstrip lines of width $W/2$. In other words, the admittance matrix of the three parallel-coupled microstrip lines is equal to two times of the admittance matrix of the two parallel-coupled microstrip lines of width $W/2$. Fig. 7 shows the normalized $J$-susceptance and electrical lengths calculated using the free computer-aided software (CAD) software TXLine for the two and three parallel-coupled microstrip lines of width $W = 0.47$ and $S = 0.189$ mm on the LTCC substrate. As expected, the new coupling scheme represented by the three parallel-coupled microstrip lines generally has a higher coupling strength. For example, the normalized $J$-susceptance is 0.65 for the new coupling scheme and 0.5 for the normal coupling scheme at 5.2 GHz. The higher coupling strength implies that the insertion loss of the dual-band bandpass filter at the 5.2-GHz band can be enhanced with the new coupling scheme. The electrical lengths for the two and three parallel-coupled microstrip lines have linear frequency dependence.

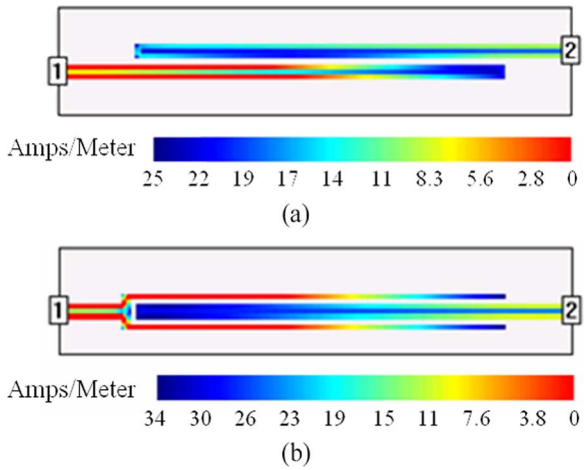


Fig. 8. Current distributions: (a) along the normal parallel-coupled lines and (b) along the novel dual-finger lines. (Color version available online at http://ieeexplore.ieee.org.)

In the above analysis, the discontinuities in the new dual-finger coupling structure are ignored for simplicity. A full-wave electromagnetic (EM) simulation can take the discontinuities into account. Fig. 8 shows the simulated current distributions along the normal and new coupling structures in Sonnet. It is seen that the current on a line is not equally distributed along the width of the line. The maximum current is on the edge of the line and gradually reducing toward the center of the line. Therefore, the coupling strength is mainly affected by the edge current. The edge current in the line of the normal coupling scheme is less than that in the line of the new coupling scheme. This is because the width of the finger lines is smaller than the width of the normal parallel-coupled lines. In this case, the maximum current or the edge current in the parallel-coupled line is 25 A/m, whereas in the finger line it is 34 A/m. Moreover, the edge current at an outer edge of the parallel-coupled line is not effective in coupling. This degrades the coupling efficiency of the normal coupling scheme. On the other hand, in the new coupling scheme, the edge currents on both fingers are effective for coupling.

Fig. 9 shows the layout and a photograph of the improved dual-band bandpass filter. Note that the new coupling scheme is only applied to the input/output ports of the filter where the coupling strength is required to be much larger than the other stages of the filter. This is also to avoid an unnecessary additional complexity to the filter structure. Fig. 10 shows the simulated and measured results. It is seen that the measured and simulated performances are in good agreement. It is found the new coupling scheme has improved the insertion loss to less than 2 dB at the 5.2-GHz band. As shown, the insertion losses are 1.25 and 1.87 dB, and return losses are 29 and 40 dB at 2.4 and 5.2 GHz, respectively. The return loss is less than −10 dB in the frequency ranges of 2.2–2.6 and 4.86–5.5 GHz. The 3-dB bandwidths are 0.5 GHz from 2.16 to 2.66 GHz and 0.66 GHz from 4.82 to 5.48 GHz. Therefore, the relative −10-dB bandwidths are 16.7% and 12.3%, and the relative −3-dB bandwidths are 21% and 12.7% at 2.4 and 5.2 GHz, respectively.

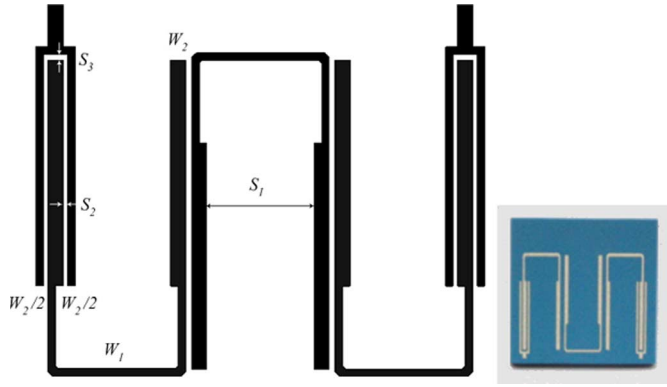


Fig. 9. Novel improved dual-band bandpass filter where $W_1 = 0.236$ mm, $W_2 = 0.47$ mm, $S_1 = 3.6$ mm, $S_2 = 0.189$ mm, $S_3 = 0.2$ mm, and the whole footprint $< 15 \times 13$ mm$^2$. (Color version available online at http://ieeexplore.ieee.org.)

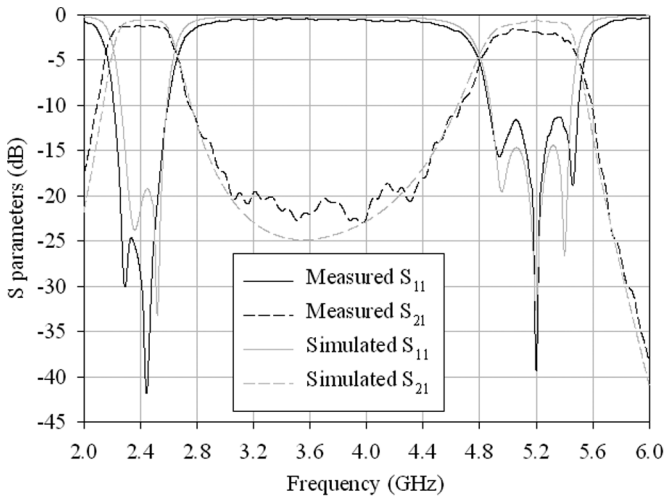


Fig. 10. Simulated and measured frequency responses of the improved dual-band bandpass filter.

## III. Integration of the Dual-Band Bandpass Filter on a Ceramic Ball Grid Array Package

Most dual-band microstrip bandpass filter reported thus far are discrete. They are large for dual-band radio transceivers operating below 6 GHz. Here, we investigate the integration of the dual-band microstrip bandpass filter on a ceramic ball grid array package, which is in line with the single-package solution of dual-band radio transceivers. The integration is analyzed with an emphasis on the connection of the dual-band filter to the external antenna and to the carried dual-band radio transceiver die. Fig. 11 shows the ceramic ball grid array package. It consists of three cofired laminated ceramic layers with a bare chip cavity formed by the middle and bottom layers. There are two buried layers and one top-layer metallization in the construction. The lower buried layer provides the metallization for the signal paths, while the upper buried layer provides the metallization for the cavity ground plane. The filter is realized with top-layer metallization. A radio transceiver die is attached upside down to the cavity ground plane. The input and output terminals of the die are connected to the external solder balls through the bond wires, signal traces, and vias. The bare chip

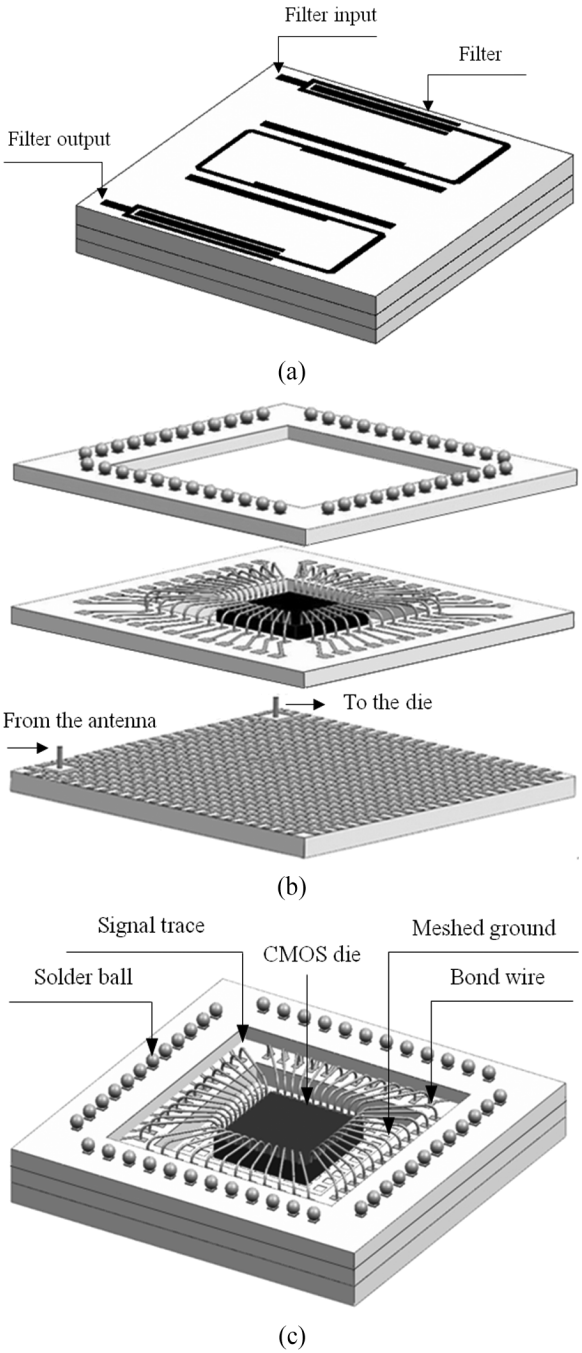


Fig. 11. Integrated dual-band bandpass filter. (a) Top view. (b) Explored view. (c) Bottom view.

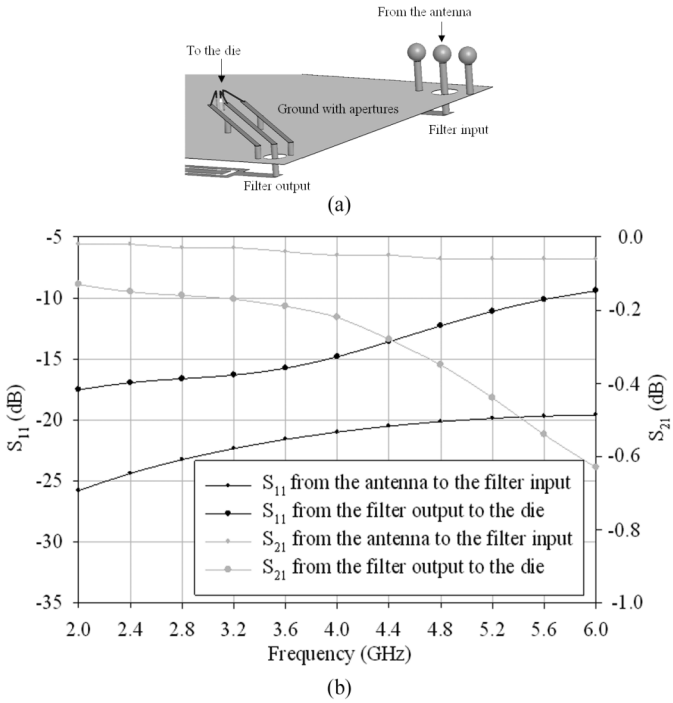


Fig. 12. Connection networks. (a) Zoom-in view of the bond wires, signal traces, vias, and solder balls. (b) Simulated $S_{11}$ and $S_{21}$.

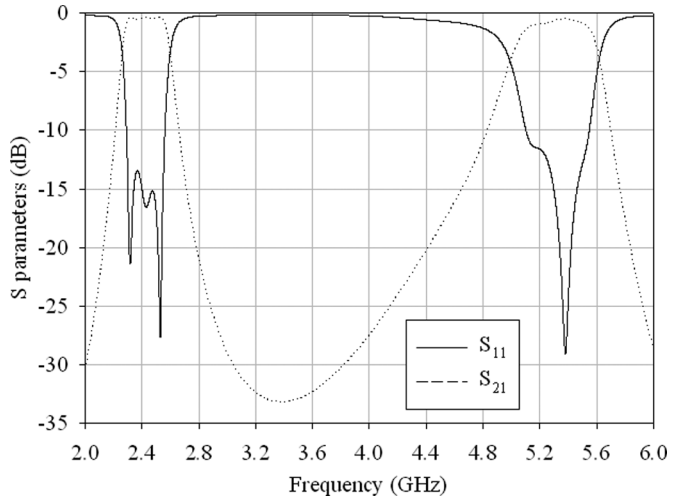


Fig. 13. Simulated frequency responses of the integrated dual-band bandpass filter where $W_1 = 0.236$ mm, $W_2 = 0.47$ mm, $S_1 = 3.6$ mm, and $S_2 = 0.5$ mm, and the whole footprint $< 15 \times 13$ mm$^2$.

is shielded from the filter by the cavity ground plane. The filter is linked to the bare chip through vias, signal traces, and bond wires and to the external antenna through vias and solder balls in a ground–signal–ground configuration. The advantage of the integrated filter is quite obvious. It offers the possibility to combine a filter with a radio transceiver die into a standard surface-mounted device. Thus, the system-level board space and the system-level manufacturing can be reduced and facilitated, respectively. Furthermore, the filter has much shorter distance to the RF output of the transceiver than a conventional filter. This implies a smaller transmission loss, which can be translated as an improvement to the filter insertion loss by a few percent.

Based on the concept described above, the dual-band bandpass filter integrated on a thin 48-ball custom-designed ceramic ball grid array package in LTCC has been simulated. The ceramic ball grid array package has dimensions of $16 \times 16 \times 1.4$ mm$^3$. A piece of silicon wafer $4 \times 4 \times 0.4$ mm$^3$ is loaded to the package cavity to model the dual-band radio transceiver die. The simulation was performed in the HFSS from Ansoft, Pittsburgh, PA. Fig. 12(a) shows the connection of the dual-band filter to the external antenna and to the carried dual-band radio transceiver die using bond wires, signal traces, and vias. The bond wire presents high impedance; it has high inductance and low capacitance. Keeping the length of the

TABLE I
COMPARISON OF 2.4- AND 5.2-GHz BANDPASS FILTER DESIGNS

| Filter in | | Ref.[3] | Ref.[5] | Ref. [8] | This work | |
|---|---|---|---|---|---|---|
| | | | | | Discrete (measured) | Integrated (simulated) |
| Technology | | Multi-layer LTCC ($\varepsilon_r$=5.9) | Rogers RO3003 ($\varepsilon_r$=3) | Rogers 6010LM ($\varepsilon_r$=10.8) | Single-layer LTCC ($\varepsilon_r$=7.8) | |
| Elements | | Ls &Cs | stepped impedance resonators & coupled microstrip lines | stepped impedance resonators & parallel-coupled microstrip lines | stepped impedance resonators & parallel-coupled microstrip lines | |
| Insertion loss (dB) | @2.4 GHz | >2.35 | 2.8 | 2 | 1.25 | 0.42 |
| | @5.2 GHz | >1.72 | 3.3 | 2.6 | 1.87 | 0.91 |
| Shape factor | @2.4 GHz | ~2.94 | ~2.13 | ~4 | 2.5 | 2.5 |
| | @5.2 GHz | ~2.63 | ~2.63 | ~4 | 2.1 | 2.4 |
| Volume ($mm^3$) | | ~5.46×5.6 ×0.94 | ~54×60×0.51 | ~5×60×0.635 | < 15×13×1 | 15×13×0.6 |

bond wire to a minimum is critical to minimize its disruptive effect on the electrical signal. Using the largest diameter wire possible is also important. In this design, we are using 40-$\mu$m wire. We place a ground wire on each side of the signal wire. This improves the situation by providing a return path in close proximity to the wire and, thus, reducing inductance slightly. The signal trace can provide the best electrical performance of the feeding network. It is primarily a coplanar waveguide. The signal integrity is well preserved. However, there is some level of loss due to dielectric material that is surrounding the conductor. As such, the length of this section does have an effect on the overall electrical behavior, but it is much less damaging than is the bond wire. The via is a transition from the signal trace to the microstrip line through an aperture on the ground plane. The diameter of the aperture has the potential to impact the electrical signal and is 0.7 mm [12]. The electrical performance of the connection networks is shown in Fig. 12(b). As can be seen, $S_{11}$ is lower than $-10$ dB and $S_{21}$ is above $-0.6$ dB in the frequency range of 2.0–5.6 GHz, which indicates that the connection provides an acceptable electrical performance over the designed frequency range.

Fig. 13 shows the final integration results of the dual-band bandpass filter. It is seen that the insertion losses are 0.42 and 0.91 dB, and $S_{11}$ is $-15$ and $-12$ dB at 2.4 and 5.2 GHz, respectively. The 3-dB bandwidths are 0.34 GHz from 2.26 to 2.6 GHz and 0.62 GHz from 5 to 5.62 GHz. Therefore, the relative 3-dB bandwidths are 14.2% and 12% at 2.4 and 5.2 GHz, respectively. The integrated bandpass filter has even better performance than the discrete one.

Table I compares the bandpass filter designs at 2.4 and 5.2 GHz in references with this work in terms of insertion loss, shape factor (the ratio between the 20- and 3-dB bandwidths), and volume. It clearly shows that the bandpass filter designed in this study is superior to those reported in references.

## IV. CONCLUSION

A microstrip bandpass filter using stepped-impedance resonators with two new coupling schemes was designed, fabricated, and tested in LTCC technology for dual-band applications at 2.4 and 5.2 GHz. It was shown that the measured and simulated performances are in good agreement. The prototype of the bandpass filter achieved the insertion loss of 1.25 and 1.87 dB, $S_{11}$ of $-29$ and $-40$ dB, and bandwidth of 21% and 12.7% at 2.4 and 5.2 GHz, respectively. The bandpass filter was further studied for a single-package solution of dual-band radio transceivers. The bandpass filter was, therefore, integrated into a ceramic ball grid array package. The integration was analyzed with an emphasis on the connection of the bandpass filter to the antenna and to the transceiver die. The integrated dual-band bandpass filter showed even better performance.

## ACKNOWLEDGMENT

The authors would like to thank K. M. Chua, Singapore Institute of Manufacturing Technology, Singapore, for his help in fabricating the filter.

## REFERENCES

[1] H. Miyake, S. Kitazawa, T. Ishizaki, T. Yamada, and Y. Nagatomi, "A miniaturized monolithic dual band filter using ceramic lamination technique for dual mode portable telephones," in *IEEE MTT-S Int. Microw. Symp. Dig.*, Jun. 1997, vol. 2, pp. 789–792.

[2] Y. X. Guo, L. C. Ong, M. Y. W. Chia, and B. Luo, "Dual-band bandpass filter in LTCC," in *IEEE MTT-S Int. Microw. Symp. Dig.*, Jun. 2005, [CD ROM], 4 pp.

[3] C. Quendo, E. Rius, and C. Person, "An original topology of dual-band filter with transmission zeros," in *IEEE MTT-S Int. Microw. Symp. Dig.*, Jun. 2003, vol. 2, pp. 1093–1096.

[4] H. M. Lee, C. M. Tsai, and C. C. Tsai, "Transmission-line filter design with fully controllable second passband," in *IEEE MTT-S Int. Microw. Symp. Dig.*, Jun. 2005, [CD ROM], 4 pp.

[5] C. M. Tsai, H. M. Lee, and C. C. Tsai, "Planar filter design with fully controllable second passband," *IEEE Trans. Microw. Theory Tech.*, vol. 53, no. 11, pp. 3429–3439, Nov. 2005.

[6] A. Apriyana, "Design of stepped impedance resonator bandpass filter for concurrent dual-band radio transceivers," M.S. thesis, Div. Circuits Syst., School Elect. Electron. Eng., Nanyang Technol. Univ., Singapore, 2003.

[7] J. T. Kuo and E. Shih, "Microstrip stepped-impedance resonator bandpass filter with an extended optimal rejection bandwidth," *IEEE Trans. Microw. Theory Tech.*, vol. 51, no. 5, pp. 1554–1559, May 2003.

[8] S. Sun and L. Zhu, "Coupling dispersion of parallel coupled microstrip lines for dual-band filters with controllable fractional pass bandwidths," in *IEEE MTT-S Int. Microw. Symp. Dig.*, Jun. 2005, [CD ROM], 4 pp.

[9] M. Makimoto and S. Yamashita, *Microwave Resonators and Filters for Wireless Communications-Theory and Design*. Berlin, Germany: Springer-Verlag, 2001.

[10] M. S. Tong, M. W. Yang, Q. S. Cao, H. S. Kim, Y. L. Lu, Y. C. Chen, and T. G. Chang, "Design and analysis of integrated-circuit package antenna (ICPA) for dual-band wireless transceivers," *Int. J. RF Microw. Comput.-Aided Eng.*, vol. 16, no. 3, pp. 250–258, May 2006.

[11] G. L. Matthaei, L. Young, and E. M. T. Jones, *Microwave Filter, Impedance-Matching Networks, and Coupling Structures*. Norwood, MA: Artech House, 1980.

[12] R. Emigh, "Electrical design for high data rate signals in conventional BT based PBGA substrates using wire bonded interconnection," in *Proc. Electron. Packag. Technol. Conf.*, Singapore, Dec. 2003, pp. 517–522.

**Yue Ping Zhang** received the B.E. and M.E. degrees from the Taiyuan Polytechnic Institute and Shanxi Mining Institute, Taiyuan University of Technology, Shanxi, China, in 1982 and 1987, respectively, and the Ph.D. degree from the Chinese University of Hong Kong, Hong Kong, in 1995, all in electronic engineering.

From 1982 to 1984, he was with the Shanxi Electronic Industry Bureau. From 1990 to 1992, he was with the University of Liverpool, Liverpool, U.K. From 1996 to 1997, he was with the City University of Hong Kong. He has taught at the Shanxi Mining Institute (1987–1990) and the University of Hong Kong (1997–1998). In 1996, he became a Full Professor with the Taiyuan University of Technology. He is currently an Associate Professor with the School of Electrical and Electronic Engineering, Nanyang Technological University, Singapore. His research interests include propagation of radio waves, characterization of radio channels, miniaturization of antennas, design of radio-frequency integrated circuits (RFICs), and implementation of wireless communications systems. His work has been widely published in the field of radio science and technology across seven IEEE societies. He is listed in Marquis' *Who's Who, Who's Who in Science and Engineering*, and *Cambridge IBC 2000 Outstanding Scientists of the 21st Century*. He serves on the Editorial Board of the *International Journal of RF and Microwave Computer-Aided Engineering* and was a Guest Editor of the journal for its "Special Issue on RF and Microwave Subsystem Modules for Wireless Communications."

Prof. Zhang serves on the Editorial Boards of the IEEE TRANSACTIONS ON MICROWAVE THEORY AND TECHNIQUES and the IEEE MICROWAVE AND WIRELESS COMPONENTS LETTERS. He has delivered scores of invited papers/keynote address at international scientific conferences. He has organized/chaired dozens of technical sessions of international symposia. He was the recipient of the 1990 Sino-British Technical Collaboration Award for his contribution to the advancement of subsurface radio science and technology and the 2000 Best Paper Award presented at the Second International Symposium on Communication Systems, Networks and Digital Signal Processing, Bournemouth, U.K. He was also the recipient of a William Mong Visiting Fellowship presented by the University of Hong Kong in 2005.

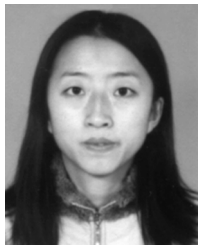

**Mei Sun** was was born in Gansu, China, in 1980. She received the B.E. degree in electrical and information engineering from Hunan University, Hunan, China, in 2000, the M.E. degree in electronic engineering from the Beijing Institute of Technology, Beijing, China, in 2003, and is currently working toward the Ph.D. degree in electrical and electronic engineering at Nanyang Technological University, Singapore.

Her research interests include intra- and inter-chip RF wireless communication system simulation and implementation and integrated antenna design for wireless communication.